Biological and Molecular Mechanisms of Sulfur Mustard Analogue-Induced Toxicity in JB6 and HaCaT Cells: Possible Role of Ataxia Telangiectasia-Mutated/Ataxia Telangiectasia-Rad3-Re...

ARTICLE *in* CHEMICAL RESEARCH IN TOXICOLOGY · JUNE 2010

Impact Factor: 3.53 · DOI: 10.1021/tx100038b · Source: PubMed

5 AUTHORS, INCLUDING:

Neera Tewari-Singh
University of Colorado
24 PUBLICATIONS **507** CITATIONS
SEE PROFILE

Carl W White
University of Colorado
171 PUBLICATIONS **6,469** CITATIONS
SEE PROFILE

Published in final edited form as:
Chem Res Toxicol. 2010 June 21; 23(6): 1034–1044. doi:10.1021/tx100038b.

Biological and molecular mechanisms of sulfur mustard analog-induced toxicity in JB6 and HaCaT cells: Possible role of ATM/ATR-cell cycle checkpoint pathway

Neera Tewari-Singh[†], **Mallikarjuna Gu**[†], **Chapla Agarwal**[†], **Carl W. White**[‡], and **Rajesh Agarwal**[†,*]

[†] Department of Pharmaceutical Sciences, School of Pharmacy, University of Colorado Denver, Aurora, CO 80045, USA

[‡] Department of Pediatrics, National Jewish Health, Denver, CO 80206, USA

Abstract

Effective medical treatment and preventive measures for chemical warfare agent sulfur mustard (HD)-caused incapacitating skin toxicity are lacking, owing to limited knowledge of its mechanism of action. The proliferating basal epidermal cells are primary major sites of attack during HD-caused skin injury. Therefore, employing mouse JB6 and human HaCaT epidermal cells, here we investigated the molecular mechanism of HD analog, 2-chloroethyl ethyl sulfide (CEES)-induced skin cytotoxicity. As compared to control, up to 1 mM CEES treatment of these cells for 2, 4 and 24 h, caused dose-dependent decreases in cell viability and proliferation as measured by DNA synthesis, together with S and G2-M phase arrest in cell cycle progression. Mechanistic studies showed phosphorylation of DNA damage sensors and checkpoint kinases, ATM at ser1981 and ATR at ser428 within 30 min of CEES exposure, and modulation of S and G2-M phase-associated cell cycle regulatory proteins which are downstream targets of ATM and ATR kinases. Hoechst-propidium iodide (PI) staining demonstrated that CEES-induced cell death was both necrotic and apoptotic in nature and latter was induced at 4 and 24 h of CEES treatment in HaCaT and JB6 cells, respectively. An increase in caspase-3 activity and both caspase-3 and PARP cleavage coinciding with CEES-caused apoptosis in both cell lines suggested the involvement of caspase pathway. Together, our findings suggest a DNA damaging effect of CEES that activates ATM/ATR-cell cycle checkpoint signaling as well as caspase-PARP pathways leading to cell cycle arrest and apoptosis/necrosis in both JB6 and HaCaT cells. The identified molecular targets, quantitative biomarkers and epidermal cell models in this study, have the potential and usefulness in rapid development of effective prophylactic and therapeutic interventions against HD-induced skin toxicity.

Introduction

Sulfur mustard (bis (2-chloroethyl) sulfide: HD) is a chemical warfare agent that remains a major threat for both military and civilian casualties (1–3). HD is an alkylating, vesicating, cytotoxic, mutagenic, and possibly a carcinogenic agent that causes extensive tissue injuries (3–6). HD-caused skin damages include edema, blister formation, ulceration, necrosis and desquamation (3,5,7). Accordingly, enormous efforts are being made in understanding the mechanisms of HD-induced skin injury for both prophylactic and therapeutic interventions

[*]To whom correspondence should be addressed: Dr. Rajesh Agarwal, Department of Pharmaceutical Sciences, School of Pharmacy, University of Colorado Denver, 12700 E. 19th Avenue, Box C238 P-15, Research 2, Aurora, CO 80045, USA; Phone: 303-724-4055, Fax: 303-724-7266, Rajesh.Agarwal@ucdenver.edu.

(3–5,8). Basal epidermal cells of skin are the major site of attack by HD (9,10) and therefore considered an important model for both biological and molecular studies (4,10–14).

HD's foremost effect is reaction with cellular molecules, mainly nucleic acids causing DNA damage that could be a direct event or via formation of electrophilic episulfonium intermediate (15–18) and/or reactive oxygen and nitrogen species (ROS and RNS) (3,5,19,20). HD (Cl-CH_2-CH_2-S-CH_2-CH_2-Cl) is a bifunctional alkylating agent that forms cross-links (DNA-CH_2-CH_2-S-CH_2-CH_2-OH) and mono-adducts with DNA interfering with normal transcription and replication of DNA. The monofunctional HD analog, CEES (CH_3-CH_2-S-CH_2-CH_2-Cl), does not cross-link but forms similar DNA mono-adducts (DNA-CH_2-CH_2-S-CH_2-CH_3). The alkylating nature of both HD and CEES, which generates N7-guanine and N3-adenine adducts, contributes to their similar toxic properties, and therefore, less toxic CEES is extensively employed to gain insight into the mechanism of action of HD (14,17,18,21–23). As DNA damage is the major cause of genotoxicity by HD/CEES, studies in different cell models have reported various pathways and biological events that are activated and triggered by HD/CEES including ataxia telangiectasia mutated (ATM), ataxia telangiectasia-Rad3-related (ATR), poly(ADP-ribose)polymerase (PARP), p53, nuclear factor-κB, cell cycle arrest and apoptosis/necrosis (12,15,18,24,25). Consistent with this, a recent study in TK6 lymphoblastoid cells has shown that CEES-induced DNA damage was associated with p53 and Chk2 phosphorylation via both ATM and ATR kinases, and that CEES-caused DNA damage is repaired via both base excision repair (BER) and nucleotide excision repair (NER) pathways (18). Apart from activation of ATM and ATR kinases of the phospho-inositide kinases (PIK) family involved in cell cycle checkpoint signaling (26,27), DNA repair nuclear protein, PARP, also plays a major role in response to DNA damage and is an important mediator of apoptotic and/or necrotic pathway (28,29). The ability of PARP to repair DNA damage is prevented by its cleavage by caspase 3, which plays a central role in apoptotic pathway and is reported to be involved in HD/CEES-caused toxicity (30). Whereas recent studies have shown the involvement of both DNA damage and repair pathways in CEES toxicity in different cell lines, detailed role of cell cycle checkpoint activation and related signaling pathways in HD/CEES-caused epidermal cytotoxicity has not been well defined. Furthermore, relevant quantitative biomarkers need to be established in appropriate epidermal cell models, which could have the potential and usefulness in rapid development of effective prophylactic and therapeutic interventions against HD-induced skin toxicity. Accordingly, here we conducted a more comprehensive study in mouse JB6 and human HaCaT epidermal cells to investigate and define the involvement of DNA damage related checkpoint signaling pathways in CEES-caused epidermal cytotoxicity. Our results in these epidermal cell models show a DNA damaging effect of CEES that activates ATM/ATR-cell cycle checkpoint signaling as well as caspase-PARP pathway leading to cell cycle arrest and apoptosis/necrosis in both JB6 and HaCaT cells.

Experimental Procedures

Cell lines and CEES treatment of cells

JB6 cells were cultured in minimal essential medium (MEM; Gibco BRL, Grand Island, NY) containing 5% heat inactivated fetal bovine serum (FBS) and 25 μg/ml gentamycin. HaCaT cells were cultured in Dulbecco's modified Eagle medium (DMEM; Gibco BRL, Grand Island, NY) with 10% FBS and 100 U/mL penicillin G-100 μg/mL streptomycin sulfate. Both cell lines were grown under standard culture conditions at 37°C in a humidified 5% CO_2 incubator. CEES was obtained from Sigma-Aldrich Chemical Co. (St. Louis., MO) and its 1M stock solution was prepared fresh in DMSO before the treatment of cells. The reported hydrolysis of CEES in the aqueous media could form 2-hydroxyethyl sulfide, sulfonium cations, and finally some hazardous compounds such as hydrogen chloride, hydrogen sulfide, carbon monoxide, chloride fumes and 1,4-dithiane (#)[1]. As the hydrolysis

of CEES cannot be avoided, the time between its addition to the growth media and further treatment of cells was kept constant. Required amount of CEES from the stock was mixed into the cell growth media for each treatment and added to the 70–80% confluent cells immediately within 18–20s after its preparation as the half-life of CEES in aqueous solution is reportedly varied and is expected to be 44 s (temperature and media not specified) or 84 s at 20°C in water (#)[1]. Cells were treated with either DMSO (control) alone or 0.1, 0.25, 0.5 and 1 mM concentrations of CEES and studies were carried out after 2, 4 and 24 h of these treatments. Unless stated otherwise, the final concentration of DMSO in the culture medium during treatments did not increase 0.1% (v/v). All CEES preparations carried out in the continuously operated chemical and biological safety hood, and treatments were done under safety laminar hood using all required and approved personal protective equipment.

Measurement of cell viability and cell proliferation (DNA synthesis)

About 2,000 cells were plated per well in 96 well culture plates, grown overnight under standard conditions and treated with either DMSO alone or 0.1–1 mM concentrations of CEES, and MTT assay was conducted at the desired time points. Cells were incubated with 1 mg/ml of 3-(4,5-Dimethylthiazol-2-yl)-2,5-diphenyltetrazolium bromide (MTT) from Sigma-Aldrich Chemical Co. (St. Louis., MO) in serum free medium for 4 h at 37°C. After removing MTT solution and adding DMSO to the cells, absorbance was read at 540 nm using Spectra max 190-microplate reader (Molecular Devices, Sunnyvale, CA). For DNA synthesis, 5-bromo-2′-deoxy-uridine (BrdU) assay (based on measurement of thymidine analog, BrdU incorporation during DNA synthesis) was done at the desired time points using cell proliferation ELISA, BrdU (colorimertic) kit from Roche Applied Science (Indianapolis, IN), following the manual instructions. Briefly, after the above mentioned CEES treatments and 2 h before the desired time points, cells were incubated with BrdU, fixed and DNA denatured, and labeled with anti-BrdU mouse monoclonal Ab-Fab. The anti-BrdU antibody binds to the BrdU incorporated in newly synthesized cellular DNA and complexes were detected by product quantification done by measuring the absorbance at 370 nm (reference wavelength: 492 nm) using Spectra max 190 microplate reader (Molecular Devices, Sunnyvale, CA). For both assays, the blank control readings were subtracted from all the sample readings.

Morphological analysis, total cell count and cell cycle analysis

Cells were seeded in 60 mm petri dishes at the density of 5000 cells/cm^2. After reaching ~70% confluency, cells were treated with either DMSO alone or 0.1–1 mM concentrations of CEES. Cells were observed under the inverted microscope for any morphological changes and cell death (in terms of floaters and cell density), and pictures were taken using Kodak DC290 camera under light microscope and processed by Kodak Microscopy Documentation System 290 (Eastman Kodak Company, Rochester, NY). Total cell counts and cell cycle analysis were carried out in triplicate. After 2, 4 and 24 h of CEES treatment, adherent and non-adherent cells were collected, washed twice with 1X PBS and total as well as dead cells were counted using a hemocytometer by Trypan blue exclusion method. Dead cells stained intensely with Trypan blue and indicated cytotoxicity. For cell cycle analysis, after the above mentioned CEES treatments in triplicate, cells were harvested, washed twice with 1X PBS and incubated in 0.5 mL of saponin/PI (Sigma-Aldrich Chemical Co. St. Louis., MO) solution (0.3% saponin, 25 μg/ml PI, 0.1 mM EDTA, and 10 μg/mL RNase in PBS) at 4°C

[1]#, References not available in PubMed library.

1. Yang, Y.-C., Szafraniec, L.L., Beaudry, W.T., Ward, J.R. (1988). Kinetics and mechanism of the hydrolysis of 2-chloroethyl sulfides. *J Org Chem. 53* 3293–3297.
2. CEES MSDS (http://www.coleparmer.com/catalog/Msds/18572.htm).

for 24 h in the dark. Cell cycle distribution was then analyzed by flow cytometry using the FACS analysis core services of the University of Colorado Cancer Center.

Quantification of apoptotic and necrotic cell death by Hoechst-PI staining

JB6 and HaCaT cells were grown in 60 mm plates as described above, treated with either DMSO alone or required concentrations of CEES and after 2, 4 and 24 h of treatment, floating and adhered cells were collected. Cells were washed twice with 1X PBS and stained by adding 10 μl of dye containing PI (1 mg/ml) and Hoechst 33342 (1 mg/mL; Sigma chemical Co., St. Louis, MO) at a ratio of 3:1, and kept on ice till the counting was completed. Quantification of apoptotic and necrotic cells was performed in triplicate for each treatment and 200 cells per sample were counted in different fields to score for live, apoptotic and necrotic cells. Cells were observed, quantified using fluorescent microscope (Zeiss Axioscope-2 plus-HBO100, Zeiss, Jena, Germany) and pictures taken using AxioCam MRC5 camera with Axiovision Rel 4.5 software. The cells were classified as follows: (i) live cells-blue fluorescence and normal structure (Hoechst stained), (ii) early apoptotic cells-bright blue florescence and enlarged with condensed, or fragmented chromatin (Hoechst stained), (iii) late apoptotic cells-bright red (pink to white) fluorescence in the centre due to condensed chromatin (Hoechst stained) and (iv) necrotic cells-bright red fluorescence and enlarged (PI stained). For Hoechst 33342, the excitation wavelength is 350 nm and emission at 461 nm and for PI excitation is at 535 nm and emission at 617 nm. The quantitative data are presented as mean ± SEM of three independent samples per treatment showing percent live, apoptotic and necrotic cells, and all the picture composites were prepared using Adobe Photoshop 6.0 (Adobe Systems, Inc., San Jose, CA).

Caspase activity assay

Caspase-3 activity was assayed by the colorimetric protease assay Apo Target kit (BioSource International, Inc., CA, USA) following the manufacturer's procedure. Briefly, after DMSO alone and CEES treatments in triplicate, cells were collected at the desired time points and lysates prepared in cell lysis buffer (Tris-buffered saline containing detergent). About 150 μg of protein lysate per sample was mixed with 2X reaction buffer and 200 mM substrate (DEVD-*p*NA), and incubated at 37°C for 2 h in the dark. The developed color was measured at 405 nm in a 96 well Spectra max 190 microplate reader (Molecular Devices, Sunnyvale, CA), and blank reading was subtracted from each sample reading before calculation.

Western blot analysis and antibodies

Total cell lysates were prepared from cells treated at 70% confluency, with DMSO or different concentrations of CEES after the desired treatment times. Protein estimations were done via Lowry method employing Bio-Rad DC protein assay kit (Bio-Rad laboratories, Hercules, CA). For immunoblot analyses, 60, 80 or 100 μg protein per sample as required was denatured in SDS sample buffer, subjected to SDS-PAGE on 6, 8, 12, or 16% Trisglycine gels, and separated proteins were transferred onto the nitrocellulose membrane by western blotting. Membranes were blocked with 5% nonfat milk powder (w/v) in Tris-buffered saline (10 mM Tris, 100 mM NaCl, 0.1% Tween 20) for 1 h at room temperature and, as desired, probed with primary antibodies overnight at 4°C followed by peroxidase conjugated appropriate secondary antibody for 1 h at room temperature. Membranes were then subjected to enhanced chemiluminescence (Amersham, Piscataway, NJ) detection. Protein loading was confirmed by stripping and re-probing the membranes with β-actin antibody. Primary antibodies for phosphorylated and total protein used were cdc25C ser216 (HaCaT cells), chk1 ser345, chk2 thr68 and thr387, cleaved PARP (Asp214), cleaved caspase-3 (Asp175), cdc2 tyr15, total cdc2, and ATR ser428 from Cell Signaling Technology (Beverly, MA); cdc25C ser216 (JB6 cells), total cdc25C, total cdc25A, cyclin

A, cyclin B1, total chk1, total chk2, cdk2 tyr15, total cdk2, ATM and ATR from Santa Cruz Biotechnology (Santa Cruz, CA); cdc25A ser75 and chk1 ser280 from Abcam Inc. (Canbridge, MA); and ATM ser1981 from Rockland Immunochemicals (Gilvertsville, PA). All the autoradiogram/bands were scanned using Adobe Photoshop 6.0 (Adobe Systems, Inc., San Jose, CA).

Statistical analysis

The data were analyzed using the SigmaStat 2.0 software (Jandel scientific, San Rafael, CA) employing ANOVA to assess the statistical significance of difference between control and CEES-treated groups. A statistically significant difference was considered present at $p < 0.05$.

Results

CEES treatment causes morphological changes, decrease in viability, growth inhibition and decrease in DNA synthesis in JB6 and HaCaT cells

Microscopic analysis of JB6 and HaCaT cells following CEES treatment demonstrated a dose-dependent increase in the number of dead cells as compared to DMSO (control) treatment alone (Figure 1, A and B). Deceased cells, seen as rounded floating cells, were observed at 4 h and were more prominent at 24 h of CEES treatment (Figure 1A and B). With higher concentrations of 0.5 and 1 mM CEES, elongated and swollen cells were recorded at all studied time points after treatment (Figure 1A and B). As substantial CEES-induced changes in cellular morphology indicating cytotoxicity were detected via light microscopy in both the cell lines, we next quantitatively evaluated the effect of CEES on the cell viability, using MTT assay. Both cell lines showed a dose-dependent reduction in the cell viability by CEES (Figure 1C and D). At 2 h of treatment in JB6 cells, only 1 mM CEES exposure resulted in a significant ($p<0.001$) decrease in cell viability as compared to DMSO control. Treatment with higher concentrations of 0.5 and 1 mM CEES for 4 h decreased JB6 cell viability to 55 and 27% ($p<0.001$) of control, respectively (Fig. 1C). As shown in Figure 1C, 24 h CEES treatment at 0.1, 0.25, 0.5 and 1 mM concentrations decreased JB6 cell viability to 82, 49, 20 and 10% ($p<0.001$) of control, respectively. Treatment of HaCaT cells with higher concentrations of 0.5 and 1 mM CEES reduced the cell viability to 89 ($p<0.01$) and 69% ($p<0.001$) at 2 h, and 78 and 40% ($p<0.001$) at 4 h, respectively (Figure 1D). At 24 h of treatment, the viability of HaCaT cells was 86, 40 and 5% ($P<0.001$) of the control following 0.25, 0.5 and 1 mM CEES exposures, respectively (Figure 1D). Treatment with lower concentrations of CEES (0.1 and 0.25 mM) for 2 h and 4 h did not show a significant decrease in cell viability as compared to their controls in both the cell lines (Figure 1C and D).

To further quantify whether CEES-induced reduction in cell viability is associated with a reduction in total cell number, we subjected both JB6 and HaCaT cells to Trypan blue staining after CEES treatment followed by cell counting. Our results clearly show that CEES causes a dose-dependent growth inhibition and death in both cell lines. As shown in Figure 1E and F, 1 mM CEES treatment caused a significant decrease in the total number of JB6 cells at 4 h ($p<0.05$) and HaCaT cells at 2 h ($p<0.005$) and 4 h ($p<0.01$) as compared to controls. At 24 h treatment, 76 ± 1.18, 43 ± 3.03 and $15 \pm 0.49 \times 10^4$ ($p<0.001$) JB6 cells were observed with 0.25, 0.5 and 1 mM CEES concentrations as compared to $115 \pm 2.63 \times 10^4$ cells in control, respectively (Figure 1E). Treatment for 24 h in HaCaT cells recorded 145 ± 5.37 ($p<0.05$), 80 ± 0.6 and $33 \pm 2.77 \times 10^4$ ($p<0.001$) total cells following 0.25, 0.5 and 1 mM CEES exposures as compared to $168 \pm 5.13 \times 10^4$ cells in control, respectively (Figure 1F). We would like to mention here that at 24 h treatment with 1 mM CEES, very few cells could be counted as CEES caused a very strong cell death leading to cellular debris

that was not accountable. In this regard, consistent with our findings in MTT assay, higher concentrations of 0.5 and 1 mM CEES caused a dose-dependent increase in cell death ($p<0.001$) at 2, 4 and 24 h of treatments in JB6 and HaCaT cells as compared to their controls, respectively (Figure 1G and H). CEES treatment at 0.25 mM concentration also caused a significant ($p<0.001$) increase in cell death but only at 24 h in JB6 cells and at 4 and 24 h in HaCaT cells ($p<0.01$ and $p<0.001$) (Figure 1G and H).

Based on our results showing CEES inhibits cell growth, we next quantified the effect of CEES on DNA synthesis that is indicative of cell proliferation. As the chemical analogue of thymidine, 5-bromo-2′-deoxy-uridine (BrdU) is incorporated into the newly synthesized DNA strands of actively proliferating cells, we employed BrdU labeling of cells to quantify cell proliferation at DNA synthesis level. Both JB6 and HaCaT cells showed a strong anti-proliferative effect of CEES, as evidenced by a decrease in BrdU incorporation with increasing concentrations of CEES at all the time points studied (Figure 1I and J). At early treatment time of 2 h in both the cells, 0.5 and 1 mM concentrations of CEES reduced the BrdU incorporating JB6 cells to 38 and 22% ($p<0.001$) and HaCaT cells to 55 and 25% ($p<0.001$) of their controls, respectively (Fig. 1I and J). At 4 and 24 h exposures, 34 and 14% ($p<0.001$) of JB6 cells incorporated BrdU following 0.5 mM CEES treatment which further reduced to 17 and 8% ($p<0.001$) with 1 mM CEES at these time points as compared to controls, respectively (Figure 1I). Comparable treatment of 0.5 and 1 mM CEES concentrations reduced the BrdU incorporating HaCaT cells to 55 and 10% ($p<0.001$) at 4 h, and 50 and 8% ($p<0.001$) of the control at 24 h treatment, respectively (Figure 1J). Interestingly, 0.25 mM CEES concentration, that did not show a significant decrease in cell viability until 24 h treatment, did show a significant ($p<0.005$–$p<0.001$) decrease in cell proliferation at 4 h treatment which was more pronounced at 24 h in both the cell lines (Figure 1I and J). Together, these results suggest that CEES treatment in both JB6 and HaCaT cells causes an earlier and pronounced decrease in DNA synthesis, which possibly leads to a decrease in cell growth and viability.

CEES treatment causes S and G2-M phase arrest in cell cycle progression of JB6 and HaCaT cells

Next, we investigated whether CEES-caused decrease in DNA synthesis is accompanied by modulation in cell cycle progression of JB6 and HaCaT cells, which would either allocate cells for DNA repair or in case of extensive damage for apoptosis. After 2 h of CEES treatment, 52, 58 and 68% ($p<0.001$) of JB6 cell population was observed in S phase on exposure to 0.25, 0.5 and 1 mM concentrations of CEES as compared to 40% S phase cells in DMSO control, respectively (Figure 2A). Similarly, 4 h CEES treatment arrested 44, 49 and 64% ($p<0.001$) of JB6 cells in S phase compared to only 24% in control, respectively (Figure 2A). The CEES-caused S phase arrest in JB6 cells was at the expense of G2-M and/or G1 phase (Figure 2A). In HaCaT cells, 2–4 h CEES treatment at 0.25–1 mM concentrations also resulted in an increase in S phase population ($p<0.005$) but to a lesser extent as compared to JB6 cells; however, 24 h treatment caused a significant ($p<0.05$–$p<0.001$) number of cells in both S and G2-M phases as compared to controls (Figure 2B).

CEES treatment causes phosphorylation of ATM at ser1981 and ATR at ser428 in JB6 and HaCaT cells

The cell cycle checkpoints are activated in response to DNA damage and are regulated by a network of DNA-damage sensor kinases, mainly the ATM and ATR (26,27,31,32). Based on our results showing that CEES causes a strong S phase arrest together with inhibition in DNA synthesis in both JB6 and HaCaT cells, we next assessed the effect of CEES on the activation of ATM and ATR, the sensors of DNA damage or DNA replication stress and mediators of cell cycle checkpoint activation. The phosphorylation of ATM at ser1981

represents its activation and is an indicator of DNA damage related change (31). Though there are no reports on specific phosphorylation sites on ATR that represent its activation, the phosphoATR ser438 antibody demonstrates the *in vivo* and UV-induced phosphorylation of this kinase and has proved as a valuable tool for checking ATR activation as reported in a number of published studies (33–35). Since activation of these pathways is an early response following DNA damage, studies were performed starting at 30 min post CEES exposure until 4 h. Compared to DMSO control, 30 min CEES treatment of JB6 and HaCaT cells resulted in an increased phosphorylation of ATM at ser1981 and ATR at ser428; however, no significant change in the total protein was observed (Figure 3). ATM phosphorylation was not observed after 2 h of CEES treatment but ATR phosphorylation was evidenced at 2 and 4 h after CEES treatment (data not shown).

CEES treatment modulates S and G2-M phase cell cycle regulatory proteins

Based on the results showing that CEES causes S and/or G2-M phase cell cycle arrest, DNA synthesis inhibition and phosphorylation of ATM and ATR clearly suggesting a DNA damaging response, we next analyzed the alterations in cell cycle regulatory proteins, which are downstream targets of ATM/ATR activation and associated with S and/or G2-M phase. Upon their activation, ATM and ATR kinases phosphorylate chk1 and chk2 effector kinases eventually leading to cell cycle arrest for DNA repair to maintain the genome integrity (32). S phase arrest is mainly associated with chk2-cdc25A-cdk2-cyclinA pathway and G2-M with chk1/2-cdc25C/A-cdc2-cyclinB1 pathway (26,36,37). Western blot analysis of 2 and 4 h CEES-treated JB6 and HaCaT cells showed an increase in the phosphorylation of chk1 at ser345 and ser280 and chk2 at thr68 and thr387 as compared to their respective controls, without noticeable changes in total chk1 and chk2 protein levels (Figure 4A and B). We then examined whether the activation of chk1 and chk2 also induced the phosphorylation of cdc25A/C. CEES caused a strong phosphorylation of cdc25A at ser75 following 2 and 4 h of its treatment in JB6 cells (Figure 4A) and 4 h of its treatment in HaCaT cells (Figure 4B). Some degradation of this protein was also observed at 4 h of 1 mM CEES treatment in JB6 (Figure 4A) and HaCaT (Figure 4B) cells. We also observed an increase in the phosphorylation of cdc25C at ser216 within 2 h of CEES treatment as compared to control in HaCaT and JB6 cells, which persisted up to 4 h in JB6 cells. A stronger phosphorylation of cdc25A as compared to cdc25C was observed in both the cell lines (Figure 4A and B). Significant changes compared to control in these proteins were not observed at 24 h of CEES treatment (data not shown).

As the cell cycle progression is intricately mediated by the activity of CDK-cyclin complexes (26,38), we next analyzed whether CEES modulates the protein levels of cdk2, cdk1 (cdc2) and associated cyclins A, E and B1. The phosphorylation of cdc25A and cdc25C is associated with a negative regulation which leads to an accumulation of cdk2 and cdc2 phosphorylated at tyr15 that is the inactive state and leads to the arrest of cells in S and G2-M phases of cell cycle progression (26,38). Strong phosphorylation at tyr15 residue of both cdk2 and cdc2 was observed following 24 h treatment of 0.25–1 mM concentrations of CEES compared to control in both JB6 and HaCaT cells (Figure 4C and D). CEES treatment resulting in the phosphorylation of cdk2 and cdc2 was accompanied by an accumulation of cyclins A and B1 at 24 h exposure in JB6 cells (Figure 4C). In HaCaT cells, CEES treatment as above, resulted in cdk phosphorylation and a strong cyclin B1 accumulation but strong accumulation of cyclin A was not observed (Figure 4D). This observation was in accordance with a weaker S phase arrest of HaCaT cells as compared to JB6 cells. No change in cyclin E levels was seen with CEES treatment in both the cell lines (data not shown). Together, these results suggested that CEES-induced S and G2-M phase cell cycle arrests involved the modulation of respective cell cycle regulatory proteins in both JB6 and HaCaT cells.

CEES treatment of JB6 and HaCaT cells results in both apoptotic and necrotic cell death

Depending on the extent of DNA damage, DNA repair for cell cycle progression can occur during cell cycle arrest and/or apoptosis if DNA damage is severe. Accordingly, we next examined CEES effect on cell death as apoptotic and/or necrotic. Following required CEES treatments, cells were stained with Hoechst-PI and observed under fluorescence microscope using the desired filters. Data from this experiment showed that CEES treatment causes both necrotic and apoptotic cell death in JB6 and HaCaT cells. In JB6 cells, following 2 and 4 h treatment with 0.25–1 mM concentrations of CEES, very few apoptotic cells were observed though there was a significant ($p<0.05$–$p<0.001$) increase as compared to DMSO controls (Figure 5A and B). However, exposure of JB6 cells to CEES for 24 h resulted in 13 ($p<0.05$), 20 and 53% ($p<0.001$) apoptotic cells at 0.25, 0.5 and 1 mM doses as compared to 6% apoptotic cells in corresponding controls, respectively (Figure 5A). Reversely, necrotic JB6 cell population was maximum at 2 h of CEES treatment that decreased following 4 and 24 h exposures, but these cells increased in a dose-dependent manner ($p<0.05$–$p<0.001$) as compared to controls at all studied time points (Figure 5A–C). In HaCaT cells, a maximum of 23 and 54% ($p<0.001$) apoptotic cell population was observed at 4 h treatment of 0.5 and 1 mM CEES concentrations as compared to 4% apoptotic cells in control, respectively (Figure 5D–F). Though a dose-dependent increase ($p<0.005$–$p<0.001$) as compared to control of necrotic cells was seen at 2 and 4 h of CEES treatment in HaCaT cells, maximum necrotic cells were documented after 24 h of CEES treatment that also increased in a dose-dependent manner ($p<0.01$–$p<0.001$) as compared to their controls (Figure 5E). These results show that while maximum apoptotic cell death was evidenced late at 24 h of CEES treatment in JB6 cells, increase in the apoptotic cell population was seen early at 4 h treatment in HaCaT cells while maximum necrotic cells were evidenced later at 24 h exposure.

CEES-caused apoptotic cell death involves caspase-3 activation, and cleavage of both caspase-3 and PARP

Based on the Hoechst-PI staining results showing that CEES caused apoptotic cell death at 24 h in JB6 cells and at 4 h in HaCaT cells, next we assessed whether CEES activates caspase-PARP pathway, the main executors of apoptotic process. First, we measured the caspase-3 activity after treatment of JB6 and HaCaT cells with 0.25–1 mM concentrations of CEES for 2, 4 and 24 h. As speculated, an increase in caspase-3 activity ($p<0.05$ and $p<0.001$) was observed at 24 h in JB6 cells following treatments of 0.5 and 1 mM CEES concentrations as compared to DMSO control (Figure 6A). In HaCaT cells, compared to DMSO treated cells, maximum caspase-3 activity was observed at 4 h that persisted up to 12 h and decreased by 16 h treatment of 0.5 and 1 mM concentrations of CEES, respectively (Figure 6B). Based on the increase in caspase-3 activity that was observed with an increase of apoptosis in JB6 and HaCaT cells following CEES treatments, we next analyzed the presence of cleaved caspase-3 and PARP in these cells by western blotting. As seen in Figure 6C, CEES caused strong accumulation of cleaved caspase-3 and PARP following 24 h of its treatment at 0.5 and 1 mM concentrations in JB6 cells as compared to controls. Similar CEES treatment with 0.5 and 1 mM doses resulted in the cleavage of caspase-3 at 2 and 4 h and cleavage of PARP at 4 h in HaCaT cells (Figure 6D). Together, these results suggest the involvement of caspase pathway in CEES-induced apoptosis in both JB6 and HaCaT cells.

Discussion

Lack of complete understanding of mechanisms involved in HD-caused epidermal cell and skin toxicity has limited the development of its effective prophylactic and therapeutic interventions. Herein we identified a DNA damaging effect of CEES that activates ATM/

ATR-cell cycle checkpoint signaling as well as caspase-PARP pathways leading to cell cycle arrest and apoptosis/necrosis in both JB6 and HaCaT cells. Mouse epidermal JB6 cells are established skin model to translate toxic effects of test compounds in human skin (39,40). HaCaT cells are spontaneously immortalized adult human keratinocytes that carry UV characteristic mutations in both alleles of p53 but exhibit normal growth and differentiation, and are appropriate *in vitro* model to study toxic and DNA damaging effects (41,42). Our results clearly show that CEES-induced biological effects such as decrease in cell viability, DNA synthesis and S and G2-M phase cell cycle arrest were associated with the activation of DNA-damage sensor kinases ATM and ATR, and further modulation of S and G2-M phase regulatory molecules in both mouse and human epidermal cells (Figure 7). CEES-induced apoptosis in both the cell lines involved caspase-3 and PARP cleavage, confirming the activation of caspase pathway (Figure 7).

The major toxic effect of HD on skin is delayed vesication indicated by epidermal-dermal separation, accompanied by keratinocyte cell death in basal epidermal layer and an inflammatory response (43). Due to structural similarity in CEES- and HD-induced monoadducts and observed toxic effects, CEES is employed as an experimental alternative to study mechanisms of HD-induced skin toxicity (18,22,44,45). Several reports show that the cause of CEES/HD-related keratinocyte toxicity is mainly DNA damage (3–5,8,18); the role of some related molecules and mechanisms in response to DNA damage is also suggested in epidermal cells, lymphocytes and lymphoblastoid cells (12,15,18,24,25,43). Genomic analysis employing HD-treated mouse ear tissue has indicated an up regulation in apoptosis, transcription factors, cell cycle and inflammation-related genes (46,47) without detailed analysis of associated signaling pathways.

Most important biological effect of HD/CEES on skin is a decrease in cell viability (5,10), and indeed, our results showed CEES-caused epidermal cell toxicity with a decrease in cell viability and growth in both JB6 and HaCaT cells. We also found that CEES-caused decrease in DNA synthesis was much earlier and with lower doses, suggesting that this is an important event preceding cell death. Since observed decrease in DNA synthesis could be due to DNA damaging effect of CEES, we speculated the activation of cell cycle checkpoint pathway involving ATM and ATR kinases, which regulate cell cycle progression for DNA repair or in case of severe damage, apoptotic cell death (31,48,49). ATM and ATR phosphorylate chk2 and chk1 (50,51), respectively; however, recent reports suggest their overlapping activity towards chk2/1, p53 and H2A.X phosphorylation (52,53). Though, the involvement of ATM and ATR in CEES-induced injury is reported earlier (18,25),, our results further reveal their phosphorylation within 30 min of CEES treatment in both JB6 and HaCaT cells, suggesting this as an early and perhaps a detrimental event in CEES-induced DNA-damage checkpoint signaling and cell cycle arrest leading to cytotoxicity.

Previously, HD is shown to induce G1/S and G2 arrests in different human skin cell lines (25,54); however, we found that CEES causes S and G2-M arrest in both JB6 and HaCaT cells. ATM/ATR-chk2/chk1 activation phosphorylates cdc25C/A phosphatase that leads to inhibitory phosphorylation of cdk2 and cdc2 at tyr15 resulting in an inactive cdk2-cyclin A/E and cdc2-cyclin B1 complex followed by S and G2-M cell cycle arrest, respectively (26,37,55). Our results are consistent with these reports, and for the first time demonstrate that 24 h CEES treatment of JB6 and HaCaT cells induces the phosphorylation of both cdk2 and cdc2 at tyr15 and accumulation of cyclin A and B1 suggesting a disruption in cyclin-Cdk complexes for the observed S and G2-M arrests. Compared to mutant p53 harboring HaCaT cells, a stronger S phase arrest and accumulation of cyclin A as well as apoptotic cell death at later time point (24 h) were observed in JB6 cells, suggesting an important role of p53 in CEES-induced cell cycle arrest and cytotoxicity. Since ATM and chk2 could directly phosphorylate p53 (50), CEES-caused phosphorylation of both ATM and chk2 further

suggests the role of p53 in the DNA damage response of CEES. Whereas the role of p53 in CEES/HD-caused injury is reported (8,43,56), more studies are needed in future to delineate the involvement of p53-dependent pathways in CEES-caused DNA damage and associated biological outcomes.

Both JB6 and HaCaT cells with severe CEES-induced DNA damage that could not undergo repair, were alternatively eliminated via apoptotic death, which was evidenced at 24 h after CEES treatment in JB6 cells but was much earlier (at 4 h) in HaCaT cells harboring p53 mutations, again indicating the involvement of p53 in apoptotic cell death by this agent. PARP is an important player in response to DNA damage, and regulates cellular functions such as DNA repair, cell cycle progression, cell death, chromatin function (57,58). During apoptotic death, the ability of PARP to repair DNA damage is prevented following its cleavage by caspases; PARP could also trigger necrotic cell death due to rapid consumption of substrate NAD^+ leading to depletion of ATP (58). Many reports indicate that HD/CEES-related cell death involves PARP and could be both apoptotic and necrotic in nature depending on dose and time (3–5,12,13,24). Our results also showed that CEES-caused cell death involves activation of caspase-3 and PARP cleavage, and is both apoptotic and necrotic, suggesting a direct necrotic and programmed cell death following CEES-caused DNA damage and/or cell cycle arrest. HD-caused apoptosis has been shown to involve both major pathways, namely Fas-dependent death receptor (extrinsic) and mitochondrial (intrinsic) apoptotic cell death (43,59), which might also be the case in the observed CEES-caused activation of caspase-3 and apoptotic cell death in our present study; however, further studies are needed in future to address such mechanisms. Since during DNA-damaging agent induced apoptosis, ATR is reported to be cleaved by caspase-3 or -7 that in turn affects the ability of ATM to phosphorylate p53 (27), there could be a possible relation between DNA-damage sensing kinases and caspase-3 in CEES-caused apoptotic cell death that requires further insight in future.

CEES-induced DNA damage could also be repaired by both base excision repair (BER) and nucleotide excision repair (NER) (17,18), indicating both double and single strand breaks by CEES/HD. PARP plays an important role in BER, which recognizes DNA damage by DNA adduct formation and oxidative stress (18). In this study, CEES-induced activation of PARP indicates that both alkylation and oxidative stress are possibly involved in CEES-induced cytotoxicity. This is consistent with earlier studies indicating that DNA damage could occur directly via alkylation and/or via generation of ROS (3,19,60). The formation of ROS can be enhanced by depletion of glutathione (GSH) as observed by HD/CEES treatments (5,43). Together with ROS, RNS and peroxynitrite ($ONOO^-$) have also been proposed to play a major role in CEES/HD-caused cytotoxicity(20,43). The role of oxidative stress in CEES toxicity is further supported by our recent study in mouse skin showing that CEES-mediated oxidative stress plays a key role in various cellular responses leading to skin inflammation and injury (22,23). Other recent studies have also shown the involvement of oxidative stress in CEES-induced injury in both lung cells and tissue, and its reversal by an antioxidant metalloporphyrin (60,61). Together, these studies support the production and role of ROS and/or RNS in CEES-caused DNA damage as well as toxicity, and the usefulness of antioxidant therapy in attenuating HD/CEES-caused injury (60). As more detailed studies are warranted in this direction, present study provides a base for further investigations delineating the role of oxidative stress in DNA damage and activation of related signaling pathways in HD-induced skin toxicity.

Acknowledgments

The research is supported by the CounterACT Program, National Institutes of Health (NIH) Office of the Director, and the National Institute of Environmental Health Sciences (NIEHS), Grant number U54 ES015678.

Abbreviations

ATM	ataxia telangiectasia mutated
ATR	ataxia telangiectasia-Rad3-related
BrdU	5-bromo-2′-deoxy-uridine
CEES	2 chloroethyl ethyl sulfide
cdc25A	cell division cycle 25A
cdc25C	cell division cycle 25C
cdc2 (cdk1)	cell division cycle 2 kinase
cdk2	cyclin dependent kinase 2
chk	checkpoint kinase
DMSO	dimethyl sulfoxide
GSH	glutathione
HD	sulfur mustard
H2A.X	histone 2AX
MTT	3-(4,5-Dimethylthiazol-2-yl)-2,5-diphenyltetrazolium bromide
PARP	poly(ADP-ribose)polymerase
PIK	phospho-inositide kinases
ser	serine
RNS	reactive nitrogen species
$ONOO^-$	peroxynitrite
ROS	reactive oxygen species
tyr	tyrosine

References

1. Noort D, Benschop HP, Black RM. Biomonitoring of exposure to chemical warfare agents: a review. Toxicol Appl Pharmacol. 2002; 184:116–126. [PubMed: 12408956]
2. Saladi RN, Smith E, Persaud AN. Mustard: a potential agent of chemical warfare and terrorism. Clin Exp Dermatol. 2006; 31:1–5. [PubMed: 16309468]
3. Graham JS, Chilcott RP, Rice P, Milner SM, Hurst CG, Maliner BI. Wound healing of cutaneous sulfur mustard injuries: strategies for the development of improved therapies. J Burns Wounds. 2005; 4:e1. [PubMed: 16921406]
4. Kehe K, Szinicz L. Medical aspects of sulphur mustard poisoning. Toxicology. 2005; 214:198–209. [PubMed: 16084004]
5. Paromov V, Suntres Z, Smith M, Stone WL. Sulfur mustard toxicity following dermal exposure: role of oxidative stress, and antioxidant therapy. J Burns Wounds. 2007; 7:e7. [PubMed: 18091984]
6. Sawyer TW, Vair C, Nelson P, Shei Y, Bjarnason S, Tenn C, McWilliams M, Villanueva M, Burczyk A. pH-dependent toxicity of sulphur mustard in vitro. Toxicol Appl Pharmacol. 2007; 221:363–371. [PubMed: 17482225]
7. Brodsky B, Erlanger-Rosengarten A, Proscura E, Shapira E, Wormser U. From topical antidote against skin irritants to a novel counter-irritating and anti-inflammatory peptide. Toxicol Appl Pharmacol. 2008; 229:342–350. [PubMed: 18400241]
8. Ruff AL, Dillman JF. Signaling molecules in sulfur mustard-induced cutaneous injury. Eplasty. 2007; 8:e2. [PubMed: 18213398]

9. Ray R, Benton BJ, Anderson DR, Byers SL, Petrali JP. Intervention of sulfur mustard toxicity by downregulation of cell proliferation and metabolic rates. J Appl Toxicol. 2000; 20(Suppl 1):S87–91. [PubMed: 11428650]
10. Henemyre-Harris CL, Adkins AL, Chuang AH, Graham JS. Addition of epidermal growth factor improves the rate of sulfur mustard wound healing in an in vitro model. Eplasty. 2008; 8:e16. [PubMed: 18438446]
11. Kehe K, Reisinger H, Szinicz L. Sulfur mustard induces apoptosis and necrosis in SCL II cells in vitro. J Appl Toxicol. 2000; 20(Suppl 1):S81–86. [PubMed: 11428649]
12. Zhang P, Ng P, Caridha D, Leach RA, Asher LV, Novak MJ, Smith WJ, Zeichner SL, Chiang PK. Gene expressions in Jurkat cells poisoned by a sulphur mustard vesicant and the induction of apoptosis. Br J Pharmacol. 2002; 137:245–252. [PubMed: 12208782]
13. Steinritz D, Emmler J, Hintz M, Worek F, Kreppel H, Szinicz L, Kehe K. Apoptosis in sulfur mustard treated A549 cell cultures. Life Sci. 2007; 80:2199–2201. [PubMed: 17229443]
14. Han S, Espinoza LA, Liao H, Boulares AH, Smulson ME. Protection by antioxidants against toxicity and apoptosis induced by the sulphur mustard analog 2-chloroethylethyl sulphide (CEES) in Jurkat T cells and normal human lymphocytes. Br J Pharmacol. 2004; 141:795–802. [PubMed: 14769780]
15. Mol MA, van den Berg RM, Benschop HP. Proteomic assessment of sulfur mustard-induced protein adducts and other protein modifications in human epidermal keratinocytes. Toxicol Appl Pharmacol. 2008; 230:97–108. [PubMed: 18342354]
16. Kehe K, Raithel K, Kreppel H, Jochum M, Worek F, Thiermann H. Inhibition of poly(ADP-ribose) polymerase (PARP) influences the mode of sulfur mustard (SM)-induced cell death in HaCaT cells. Arch Toxicol. 2007
17. Matijasevic Z, Precopio ML, Snyder JE, Ludlum DB. Repair of sulfur mustard-induced DNA damage in mammalian cells measured by a host cell reactivation assay. Carcinogenesis. 2001; 22:661–664. [PubMed: 11285203]
18. Jowsey PA, Williams FM, Blain PG. DNA damage, signalling and repair after exposure of cells to the sulphur mustard analogue 2-chloroethyl ethyl sulphide. Toxicology. 2009; 257:105–112. [PubMed: 19111594]
19. Brimfield AA, Mancebo AM, Mason RP, Jiang JJ, Siraki AG, Novak MJ. Free radical production from the interaction of 2-chloroethyl vesicants (mustard gas) with pyridine nucleotide-driven flavoprotein electron transport systems. Toxicol Appl Pharmacol. 2009; 234:128–134. [PubMed: 18977373]
20. Korkmaz A, Yaren H, Topal T, Oter S. Molecular targets against mustard toxicity: implication of cell surface receptors, peroxynitrite production, and PARP activation. Arch Toxicol. 2006; 80:662–670. [PubMed: 16552503]
21. Choi MS, Parikh K, Saxena A, Chilukuri N. Protective effects of recombinant kunitz-domain 1 of human tissue factor pathway inhibitor-2 against 2-chloroethyl ethyl sulfide toxicity in vitro. J Burns Wounds. 2007; 7:e2. [PubMed: 17846661]
22. Tewari-Singh N, Rana S, Gu M, Pal A, Orlicky DJ, White CW, Agarwal R. Inflammatory biomarkers of sulfur mustard analog 2-chloroethyl ethyl sulfide-induced skin injury in SKH-1 hairless mice. Toxicol Sci. 2009; 108:194–206. [PubMed: 19075041]
23. Pal A, Tewari-Singh N, Gu M, Agarwal C, Huang J, Day BJ, White CW, Agarwal R. Sulfur mustard analog induces oxidative stress and activates signaling cascades in the skin of SKH-1 hairless mice. Free Radic Biol Med. 2009
24. Debiak M, Kehe K, Burkle A. Role of poly(ADP-ribose) polymerase in sulfur mustard toxicity. Toxicology. 2008
25. Kehe K, Balszuweit F, Emmler J, Kreppel H, Jochum M, Thiermann H. Sulfur mustard research-strategies for the development of improved medical therapy. Eplasty. 2008; 8:e32. [PubMed: 18615149]
26. Abraham RT. Cell cycle checkpoint signaling through the ATM and ATR kinases. Genes Dev. 2001; 15:2177–2196. [PubMed: 11544175]
27. Yang J, Xu ZP, Huang Y, Hamrick HE, Duerksen-Hughes PJ, Yu YN. ATM and ATR: sensing DNA damage. World J Gastroenterol. 2004; 10:155–160. [PubMed: 14716813]

28. Marchenko ND, Zaika A, Moll UM. Death signal-induced localization of p53 protein to mitochondria. A potential role in apoptotic signaling. J Biol Chem. 2000; 275:16202–16212. [PubMed: 10821866]
29. Dantzer F, de La Rubia G, Menissier-De Murcia J, Hostomsky Z, de Murcia G, Schreiber V. Base excision repair is impaired in mammalian cells lacking Poly(ADP-ribose) polymerase-1. Biochemistry. 2000; 39:7559–7569. [PubMed: 10858306]
30. Mol MA, van den Berg RM, Benschop HP. Involvement of caspases and transmembrane metalloproteases in sulphur mustard-induced microvesication in adult human skin in organ culture: directions for therapy. Toxicology. 2009; 258:39–46. [PubMed: 19167455]
31. Tanaka T, Kajstura M, Halicka HD, Traganos F, Darzynkiewicz Z. Constitutive histone H2AX phosphorylation and ATM activation are strongly amplified during mitogenic stimulation of lymphocytes. Cell Prolif. 2007; 40:1–13. [PubMed: 17227291]
32. Walker M, Black EJ, Oehler V, Gillespie DA, Scott MT. Chk1 C-terminal regulatory phosphorylation mediates checkpoint activation by de-repression of Chk1 catalytic activity. Oncogene. 2009; 28:2314–2323. [PubMed: 19421147]
33. Wang WH, Hullinger RL, Andrisani OM. Hepatitis B virus X protein via the p38MAPK pathway induces E2F1 release and ATR kinase activation mediating p53 apoptosis. J Biol Chem. 2008; 283:25455–25467. [PubMed: 18606816]
34. Kiziltepe T, Hideshima T, Catley L, Raje N, Yasui H, Shiraishi N, Okawa Y, Ikeda H, Vallet S, Pozzi S, Ishitsuka K, Ocio EM, Chauhan D, Anderson KC. 5-Azacytidine, a DNA methyltransferase inhibitor, induces ATR-mediated DNA double-strand break responses, apoptosis, and synergistic cytotoxicity with doxorubicin and bortezomib against multiple myeloma cells. Mol Cancer Ther. 2007; 6:1718–1727. [PubMed: 17575103]
35. Chandris P, Giannouli CC, Panayotou G, Kletsas D. Compromise in mRNA processing machinery in senescent human fibroblasts: implications for a novel potential role of Phospho-ATR (ser428). Biogerontology.
36. Nakanishi M, Shimada M, Niida H. Genetic instability in cancer cells by impaired cell cycle checkpoints. Cancer Sci. 2006; 97:984–989. [PubMed: 16925578]
37. Uto K, Inoue D, Shimuta K, Nakajo N, Sagata N. Chk1, but not Chk2, inhibits Cdc25 phosphatases by a novel common mechanism. Embo J. 2004; 23:3386–3396. [PubMed: 15272308]
38. Deep G, Singh RP, Agarwal C, Kroll DJ, Agarwal R. Silymarin and silibinin cause G1 and G2-M cell cycle arrest via distinct circuitries in human prostate cancer PC3 cells: a comparison of flavanone silibinin with flavanolignan mixture silymarin. Oncogene. 2006; 25:1053–1069. [PubMed: 16205633]
39. Dhar A, Young MR, Colburn NH. The role of AP-1, NF-kappaB and ROS/NOS in skin carcinogenesis: the JB6 model is predictive. Mol Cell Biochem. 2002; 234–235:185–193.
40. Dhanalakshmi S, Agarwal C, Singh RP, Agarwal R. Silibinin up-regulates DNA-protein kinase-dependent p53 activation to enhance UVB-induced apoptosis in mouse epithelial JB6 cells. J Biol Chem. 2005; 280:20375–20383. [PubMed: 15792956]
41. Zheng B, Hwang HM, Yu H, Ekunwe S. DNA damage produced in HaCaT cells by combined fluoranthene exposure and ultraviolet A irradiation. Environ Mol Mutagen. 2004; 44:151–155. [PubMed: 15278918]
42. Henseleit U, Zhang J, Wanner R, Haase I, Kolde G, Rosenbach T. Role of p53 in UVB-induced apoptosis in human HaCaT keratinocytes. J Invest Dermatol. 1997; 109:722–727. [PubMed: 9406811]
43. Kehe K, Balszuweit F, Steinritz D, Thiermann H. Molecular toxicology of sulfur mustard-induced cutaneous inflammation and blistering. Toxicology. 2009; 263:12–19. [PubMed: 19651324]
44. Sabourin CL, Petrali JP, Casillas RP. Alterations in inflammatory cytokine gene expression in sulfur mustard-exposed mouse skin. J Biochem Mol Toxicol. 2000; 14:291–302. [PubMed: 11083082]
45. Hayden PJ, Petrali JP, Stolper G, Hamilton TA, Jackson GR, Wertz PW, Ito S, Smith WJ, Klausner M. Microvesicating Effects of Sulfur Mustard on an In Vitro Human Skin Model. Toxicol In Vitro. 2009

46. Sabourin CL, Rogers JV, Choi YW, Kiser RC, Casillas RP, Babin MC, Schlager JJ. Time- and dose-dependent analysis of gene expression using microarrays in sulfur mustard-exposed mice. J Biochem Mol Toxicol. 2004; 18:300–312. [PubMed: 15674844]
47. Rogers JV, Choi YW, Kiser RC, Babin MC, Casillas RP, Schlager JJ, Sabourin CL. Microarray analysis of gene expression in murine skin exposed to sulfur mustard. J Biochem Mol Toxicol. 2004; 18:289–299. [PubMed: 15674843]
48. Kurose A, Tanaka T, Huang X, Halicka HD, Traganos F, Dai W, Darzynkiewicz Z. Assessment of ATM phosphorylation on Ser-1981 induced by DNA topoisomerase I and II inhibitors in relation to Ser-139-histone H2AX phosphorylation, cell cycle phase, and apoptosis. Cytometry A. 2005; 68:1–9. [PubMed: 16184611]
49. Agarwal C, Tyagi A, Agarwal R. Gallic acid causes inactivating phosphorylation of cdc25A/cdc25C-cdc2 via ATM-Chk2 activation, leading to cell cycle arrest, and induces apoptosis in human prostate carcinoma DU145 cells. Mol Cancer Ther. 2006; 5:3294–3302. [PubMed: 17172433]
50. Shiloh Y. ATM and related protein kinases: safeguarding genome integrity. Nat Rev Cancer. 2003; 3:155–168. [PubMed: 12612651]
51. Goodarzi AA, Block WD, Lees-Miller SP. The role of ATM and ATR in DNA damage-induced cell cycle control. Prog Cell Cycle Res. 2003; 5:393–411. [PubMed: 14593734]
52. Gatei M, Sloper K, Sorensen C, Syljuasen R, Falck J, Hobson K, Savage K, Lukas J, Zhou BB, Bartek J, Khanna KK. Ataxia-telangiectasia-mutated (ATM) and NBS1-dependent phosphorylation of Chk1 on Ser-317 in response to ionizing radiation. J Biol Chem. 2003; 278:14806–14811. [PubMed: 12588868]
53. Kurz EU, Douglas P, Lees-Miller SP. Doxorubicin activates ATM-dependent phosphorylation of multiple downstream targets in part through the generation of reactive oxygen species. J Biol Chem. 2004; 279:53272–53281. [PubMed: 15489221]
54. Simpson R, Lindsay CD. Effect of sulphur mustard on human skin cell lines with differential agent sensitivity. J Appl Toxicol. 2005; 25:115–128. [PubMed: 15747377]
55. Zhou BB, Elledge SJ. The DNA damage response: putting checkpoints in perspective. Nature. 2000; 408:433–439. [PubMed: 11100718]
56. Rosenthal DS, Simbulan-Rosenthal CM, Iyer S, Smith WJ, Ray R, Smulson ME. Calmodulin, poly(ADP-ribose)polymerase and p53 are targets for modulating the effects of sulfur mustard. J Appl Toxicol. 2000; 20(Suppl 1):S43–49. [PubMed: 11428642]
57. Valenzuela MT, Guerrero R, Nunez MI, Ruiz De Almodovar JM, Sarker M, de Murcia G, Oliver FJ. PARP-1 modifies the effectiveness of p53-mediated DNA damage response. Oncogene. 2002; 21:1108–1116. [PubMed: 11850828]
58. Los M, Mozoluk M, Ferrari D, Stepczynska A, Stroh C, Renz A, Herceg Z, Wang ZQ, Schulze-Osthoff K. Activation and caspase-mediated inhibition of PARP: a molecular switch between fibroblast necrosis and apoptosis in death receptor signaling. Mol Biol Cell. 2002; 13:978–988. [PubMed: 11907276]
59. Rosenthal DS, Velena A, Chou FP, Schlegel R, Ray R, Benton B, Anderson D, Smith WJ, Simbulan-Rosenthal CM. Expression of dominant-negative Fas-associated death domain blocks human keratinocyte apoptosis and vesication induced by sulfur mustard. J Biol Chem. 2003; 278:8531–8540. [PubMed: 12482751]
60. Gould NS, White CW, Day BJ. A role for mitochondrial oxidative stress in sulfur mustard analog 2-chloroethyl ethyl sulfide-induced lung cell injury and antioxidant protection. J Pharmacol Exp Ther. 2009; 328:732–739. [PubMed: 19064720]
61. O'Neill HC, White CW, Veress LA, Hendry-Hofer TB, Loader JE, Min E, Huang J, Rancourt RC, Day BJ. Treatment with the catalytic metalloporphyrin AEOL 10150 reduces inflammation and oxidative stress due to inhalation of the sulfur mustard analog 2-chloroethyl ethyl sulfide. Free Radic Biol Med. 48:1188–1196. [PubMed: 20138141]

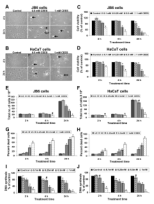

Figure 1. CEES treatment induced changes in cell morphology, dose-dependent decreases in cell viability, growth inhibition, and decrease in DNA synthesis in JB6 and HaCaT cells

JB6 and HaCaT cells were treated with DMSO (control) or with 0.1–1 mM concentrations of CEES and then examined under a light microscope for morphological analysis (A and B). After similar treatments to JB6 and HaCaT cells in 96 well plates, MTT assay (C and D) was carried out at 2, 4 and 24 h as described under 'Experimental Procedures'. At the end of each treatment time, both floaters and attached cells were collected and counted on hemocytometer after Trypan blue staining for total number of cells (E and F) and percent of dead cells (G and H) as described in the 'Experimental Procedures'. JB6 (I) and HaCaT (J) cells were treated with DMSO (control) or 0.1, 0.25, 0.5 and 1 mM concentrations of CEES for 2, 4 and 24 h in 96 well plates. At desired time points, cells were incubated with BrdU for 2 h, fixed and DNA denatured and labeled with anti-BrdU mouse monoclonal Ab-Fab. Further product quantification was done by measuring the absorbance at 370 nm (reference wavelength: 492 nm) as described under 'Experimental Procedures'. Black arrow, cell death as floating cells; white arrow, elongation of cells; black arrowhead, cell swelling; 4 h (magnification ×100), 24 h (magnification ×200). Data shown are mean ± SEM of eight independent samples for each treatment, (C and D), mean ± SEM of three independent samples for each treatment (E–H), and mean ± SEM of six independent samples for each treatment (I and J).*, $P<0.001$; ψ, $P<0.005$; $, $P<0.01$ as compared to control. UC, untreated control; VC, DMSO treated vehicle control. Similar results were obtained in two independent experiments.

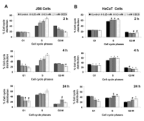

Figure 2. CEES treatment caused S and G2-M phase arrests during cell cycle progression of JB6 and HaCaT cells

JB6 (A) and HaCaT (B) cells were cultured and treated with DMSO (Control) or 0.25, 0.5 and 1 mM concentrations of CEES. Following 2, 4 and 24 h treatments, cells were collected and incubated with saponin/PI at 4°C for 24 h in the dark and subjected to FACS analysis as detailed in 'Experimental Procedures'. Data shown are mean ± SEM of three independent samples.*, P<0.001; ψ, P<0.005; $, P<0.01; #, P<0.05 as compared cells in G1, S and G2-M phases in control samples.

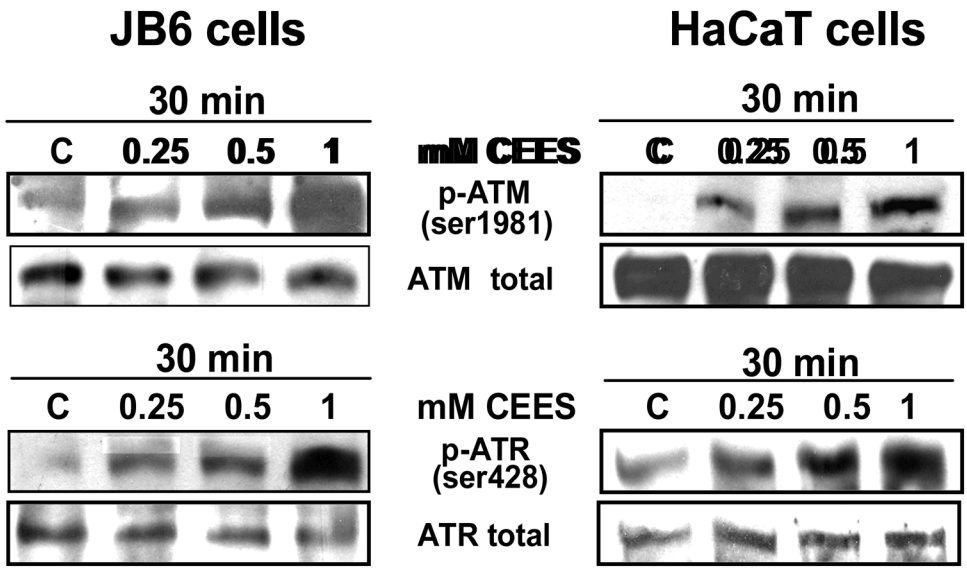

Figure 3. CEES treatment induced ATM ser1981 and/ATR ser428 phosphorylation in JB6 and HaCaT cells

JB6 and HaCaT cells were treated with DMSO (control) or 0.25, 0.5 and 1 mM concentrations of CEES, and harvested 30 min thereafter. Total cell lysates were prepared, subjected to SDS-PAGE followed by western immunoblotting with 120 μg of protein for phosphorylated ATM and ATR. Total protein levels were determined after stripping and reprobing with total ATM and ATR antibodies. C, DMSO treated control.

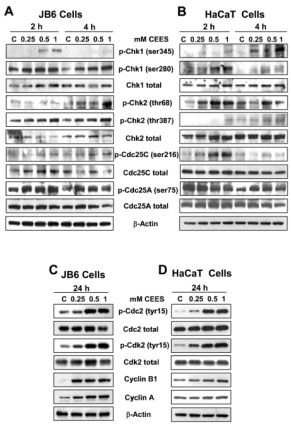

Figure 4. CEES treatment modulated the expressions of S and G2-M cell cycle regulatory proteins in JB6 and HaCaT cells

JB6 (A and C) and HaCaT (B and D) cells were treated with DMSO (control) or 0.25–1 mM concentrations of CEES and harvested at indicated time-points. Total cell lysates were prepared, subjected to SDS-PAGE followed by Western immunoblotting with 60–80 μg of protein, and membranes were probed for phosphorylated and total Chk1 and Chk2, Cdc25C and Cdc25A, Cdc2 and Cdk2, and cyclin A and B1 levels as described under ‘Experimental Procedures’. Protein loading was checked by stripping and re-probing the membranes with β-actin antibody. C, DMSO treated control.

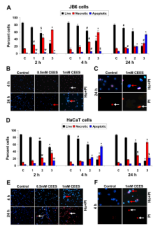

Figure 5. CEES treatment caused both apoptotic and necrotic cell death in JB6 and HaCaT cells

Cells were treated with DMSO or 0.25–1 mM concentrations of CEES for 2, 4 and 24 h. At the end of each treatment time, both floaters and attached cells were collected and stained with Hoechst+PI dye as detailed in 'Experimental Procedures', counted manually and percent live, necrotic and apoptotic cells were calculated (A and D). Cells were also observed under a fluorescence microscope and pictures were taken as detailed in 'Experimental Procedures' at magnification ×100 (B and E) and ×400 (C and F). Data shown are mean ± SEM of three independent samples. *, P<0.001; ψ, P<0.005; $, P<0.01; #, P<0.05 as compared to control. C, DMSO treated control; 1, 0.25 mM CEES; 2, 0.5 mM CEES; 3, 1 mM CEES; PI, only PI staining indicating the necrotic cells; HO+PI, Hoechst and PI staining recording both apoptotic and necrotic cells; red arrows, apoptotic cells; white arrows, necrotic cells.

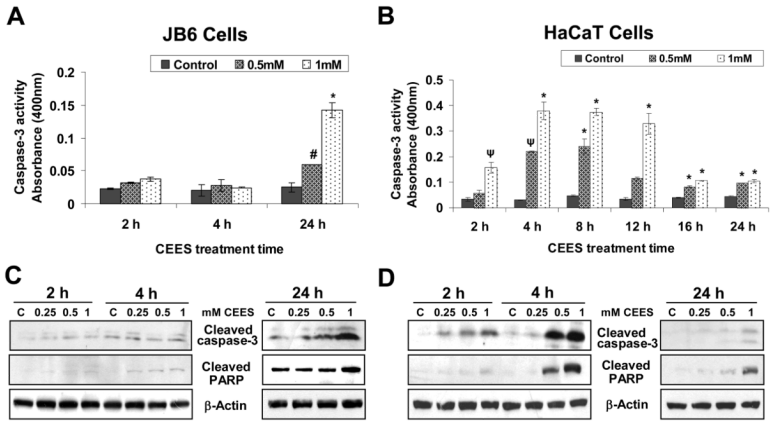

Figure 6. CEES treatment caused an increase in Caspase-3 activity and induction of Caspase-3 and PARP cleavage in JB6 and HaCaT cells

For measuring caspase-3 activity, JB6 and HaCaT cells were collected at desired time points after DMSO (control) and CEES treatments, and cell lysates prepared in the cell lysis buffer. About 150 μg of protein lysate per sample was taken and assayed (A and B) as described under 'Experimental Procedures'. For caspase-3 and PARP cleavage, JB6 and HaCaT cells were treated with DMSO (control) or 0.25, 0.5 and 1 mM concentrations of CEES and harvested at indicated time-points. Total cell lysates were prepared, subjected to SDS-PAGE followed by western immunoblotting with 80 μg of protein lysate, and membranes were probed for cleaved caspase-3 and PARP (C and D) as described under 'Experimental Procedures'. Protein loading was checked by stripping and reprobing the membranes with β-actin antibody. Data shown in A and B are mean ± SEM of three independent samples. *, $P<0.001$; ψ, $P<0.005$; #, $P<0.05$ as compared to control; C, DMSO treated control.

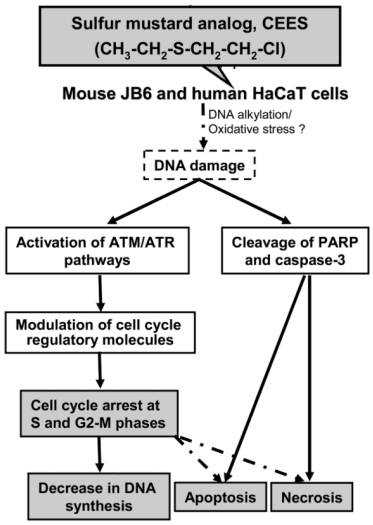

Figure 7. Proposed mechanism of CEES-caused molecular alterations leading to the observed biological events in JB6 and HaCaT cells

Our results indicate that CEES-induced decrease in cell viability and DNA synthesis, and S and G2-M phase cell cycle arrest were associated with a DNA damage followed by the activation of DNA-damage sensor kinases ATM and ATR, and modulation of S and G2-M phase regulatory molecules in both JB6 and HaCaT cells. In addition, CEES-induced apoptosis/necrosis in both cell lines was associated with cleavage of caspase-3 and PARP.